Dicle University
Journal of Engineering
https://dergipark.org.tr/tr/pub/dumf
duje.dicle.edu.tr

Research Article

# Forming Analysis of an Inner Tie-Rod End Stud Using Finite Element Modeling and Experiments

**Sait Özmen Eruslu[1*], Elçin Kahraman[2], Kürşat Kölemen[3]**

[1]Tekirdağ Namık Kemal University, Çorlu Faculty of Engineering, Department of Mechanical Engineering, oeruslu@nku.edu.tr

Orcid No: 0000-0003-2942-378X

[2] SIO Automotive Car Spare Parts Factory, Ergene/Türkiye, e.kahraman@sio-automotive.com, Orcid No: 0009-0001-0251-3008

[3] SIO Automotive Car Spare Parts Factory, Ergene/Türkiye, k.kolemen@sio-automotive.com, Orcid No: 0009-0001-0579-4300

ARTICLE INFO

*Article history*:

Received 6 January 2026
Received in revised form
27 February 2026
Accepted 5 March 2026
Available online 26 March 2026

*Keywords*:

*Inner Tie Rod End Stud, Forming Analysis, Residual Stress Analysis, Plastic Residual Strains, Elastoplastic Finite Element Analysis (FEA).*

*Doi: 10.24012/dumf.1848105*

* Corresponding author

ABSTRACT

This study presents the finite element modeling of the forming process of an inner tie-rod end stud, complemented by experimental tests. Three inner tie-rod end stud designs made from two materials, SAE 1040 and 16MnCr5, were analyzed using both numerical and experimental methods. A nonlinear, displacement-based modeling technique is employed to simulate the stud closing operation, incorporating the material's multilinear isotropic hardening behavior. This study examines the effects of expansion during the forming of a tie-rod end stud in three different designs, with a focus on residual stresses and their impact on material behavior. Residual plastic strains are identified as a key factor contributing to material expansion in the wrench sections. The material hardening rate, reduced ductility after loading, and yield strength are also important parameters affecting the results. The hardness increases due to strain hardening in both 16MnCr5 and SAE 1040 steels, whereas the observed material expansion is primarily associated with residual plastic deformation and strain hardening effects, with microstructural differences showing no significant influence on the expansion behavior. The results indicate that no material expansion is observed in 16MnCr5 due to its higher yield strength and limited residual plastic strains in the critical wrench zone, in contrast to SAE 1040 steel. In comparison with the conventional inner tie-rod end stud, the wrench-flat length has a significant effect on material expansion due to the residual stresses concentrated at the sharp corners. Furthermore, the study establishes a direct relationship between strain localization, residual plastic strain evolution, and dimensional accuracy, while demonstrating that a wrench-size-based design modification can effectively reduce forming-induced expansion.

## Introduction

A tie-rod end is an essential component of a vehicle's steering system. It connects the steering linkage to the steering knuckle, enabling the transmission of steering input to the wheel assembly and ensuring directional stability of the vehicle [1]. The outer tie-rod end is coupled to an adjusting sleeve that allows precise adjustment of the tie-rod length to set the vehicle's toe angle [2]. Inner tie-rods connect directly to the steering rack and transmit steering motion to the outer tie-rods through ball-and-socket studs, commonly incorporating polyoxymethylene (POM) elements to ensure smooth articulation.

Previous research on tie-rod systems has predominantly focused on structural performance and failure mechanisms under service conditions. Ikechukwu et al. investigated tie-rod failure through rigid-body dynamics simulations of suspension forces [3]. Fatigue damage, stress concentration in threaded regions, and compressive overload have been identified as primary failure causes [2, 4]. Koh examined low-cycle fatigue failures and estimated fatigue life experimentally and numerically using finite element methods [5]. Ozsoy et al. analyzed stress variations in tie-rod ends under different loading scenarios using FEM [6]. It is well established that the forces transmitted through tie-rods are predominantly compressive [7], particularly under adverse road conditions such as bumps and potholes, where repeated loading may promote fatigue fracture [8].

Axial forces arising during steering torque transmission are mainly compressive, making buckling resistance a critical design parameter [9]. The threaded connection between inner and outer tie-rod ends makes the rod geometry and cross-sectional properties essential for ensuring sufficient strength and stability [10-11]. Consequently, several studies have investigated stress distribution, buckling behavior, and natural frequencies of tie-rod assemblies [1,10,12]. Multibody dynamic simulations combined with finite element analysis have been used to estimate operational loads and evaluate tensile, compressive, and buckling stresses under realistic driving conditions [13-14]. In recent years, topology optimization studies have further aimed to reduce component weight while maintaining structural strength and fatigue resistance [15]. Although previous studies provide comprehensive insight into service loading,

fatigue behavior, and structural optimization, the existing literature primarily addresses the in-service performance of tie-rod assemblies rather than the manufacturing stage of individual components. In practice, tie-rod bodies are commonly produced by forging or casting, whereas ball-stud sections are manufactured through cold forming to achieve refined grain structures and improved mechanical strength. Since cold forming involves plastic deformation beyond the elastic limit, it constitutes a highly nonlinear process governed by material hardening, contact interaction, and geometric nonlinearity.

Finite element analysis is widely employed to simulate forming processes due to its capability to capture material and geometric nonlinearities as well as contact behavior [16–19]. In forming simulations, both implicit and explicit solution strategies are adopted. The implicit approach provides improved numerical stability and accuracy in predicting springback, residual stresses, and contact effects, whereas the explicit method is efficient for highly dynamic forming operations [20]. Cold working introduces severe plastic deformation, increasing dislocation density and elongating grains along the forming direction [21-22]. This microstructural evolution increases hardness while reducing ductility, thereby influencing strain localization and residual stress development.

Residual stresses originate from non-uniform plastic deformation and incomplete elastic recovery during unloading [16, 23]. They are commonly retained in components after manufacturing processes such as forging, machining, heat treatment, or cold forming, and may significantly affect dimensional accuracy and fatigue performance [24]. The magnitude of residual stresses is strongly influenced by the material hardening rate, since higher hardening constrains elastic recovery and promotes stress accumulation during unloading [25]. While residual stress and springback phenomena have been extensively modeled using elastic–plastic formulations [26–28], these investigations are generally conducted in sheet forming or generic forming contexts rather than in steering system components.

Although previous studies on tie-rod links and steering mechanisms have extensively focused on fatigue behavior, operational stresses, and stress concentrations in threaded regions, limited attention has been given to the cold forming stage of the inner tie-rod end stud and the residual stress–driven dimensional deviations arising during manufacturing. In particular, forming-induced axial expansion, plastic strain localization at wrench-flat transitions, and their dependence on material hardening and geometric design parameters remain insufficiently understood, while the coupling between forming mechanics, residual stress evolution, and post-forming dimensional accuracy has not been systematically addressed.

In this context, the present study presents a comprehensive numerical and experimental investigation of the cold forming process of the inner tie-rod end stud, with particular emphasis on the interaction between forming mechanics and dimensional accuracy. A nonlinear implicit Finite Element Analysis (FEA) incorporating material and contact nonlinearities through an isotropic hardening model is employed to predict plastic deformation, residual stress evolution, and axial expansion during unloading. To support the numerical findings, microstructural characterization and microhardness measurements are conducted to capture strain localization and hardening behavior induced by cold working. The integrated approach enables the identification of a direct linkage between forming-induced plastic strain localization, residual stress evolution, and post-forming axial expansion in the inner tie-rod end stud, while simultaneously clarifying the influence of material selection and wrench-section geometry on deformation behavior. Furthermore, the results demonstrate that wrench-size-based geometric modification can effectively mitigate forming-induced dimensional deviation, thereby providing practical insight for manufacturing-oriented design optimization and process control.

## Forming of Inner Tie-Rod End Stud

The inner tie-rod end stud is a key component of a vehicle's steering mechanism, serving as the connection between the inner and outer tie-rod ends, as shown in Figure 1.

Figure 1. Formed inner tie-rod end stud

A forming press with a capacity of 5 tons is used in the cold forming process. The forming mold is shown in Figure 2. The forming displacement is determined based on the ball rolling conditions, as the motion of the inner tie-rod end ball allows for steering angle changes. Controlled rolling reduces friction, enhances steering smoothness, and increases the component's service life. The study focuses on the finite element modeling of the forming process of the inner tie-rod end stud.

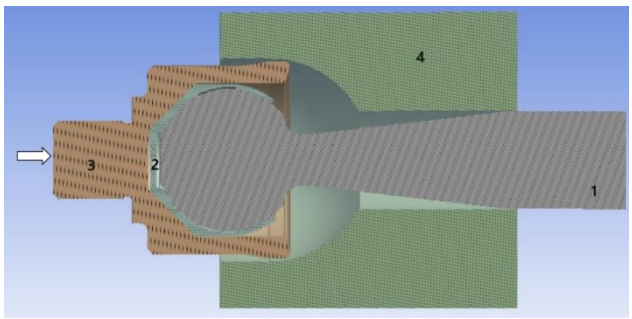


Figure 2. Forming a mold model of the inner tie-rod

end stud Here, 1 – Inner tie-rod end; 2 – POM bearing; 3 – Inner tie-rod end stud; 4 – Inner tie-rod end stud forming mould.

This study aims to investigate the effects of the forming process on residual plastic strains and strain hardening in two materials and to evaluate the influence of a wrench-size-based design, as shown in Figure 3.

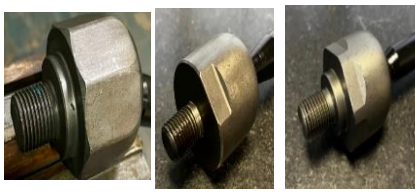

a) b) c)

Figure 3. Wrench size–based designs a) Design 1 b) Design 2 c) Design 3

## Measurement Controls After Forming

In serial production, the wrench flat size and peak dimension of the inner tie-rod end stud are critical for ensuring reliable disassembly and for accurately controlling the applied tie-rod torque during assembly operations. To verify dimensional accuracy, the wrench flat size and peak size of the inner tie-rod end stud are measured using a caliper on the formed studs, as shown in Figure 4.

Due to the excessive expansion observed at the peak dimensions, dimensional measurements of the inner tie-rod end stud for Design 2 and Design 3 were conducted exclusively using Material 1. In addition, the inner diameter was measured to enable precise adjustment of tie-rod torque and forming displacement. Torque calculations were performed using the instrument illustrated in Figure 5.

a) b) c) d)

Figure 4. Dimensional measurement of the inner tie-rod end stud for Design 1: a) Wrench flat size for material 1, b) Peak size for material 1, c) Wrench flat size for material 2, d) Peak size for material 2

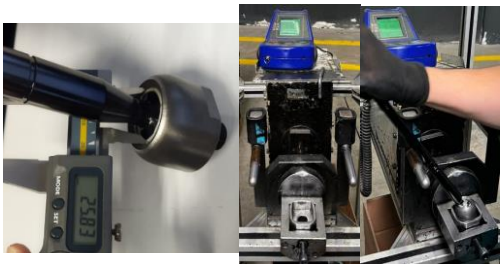

a) b)

Figure 5. Measurement control of the inner tie-rod end stud a) Inner dimension size b) Controlling torque equipment

## Finite Element Model

The forming process of the inner tie-rod end stud is performed using the implicit finite element analysis method. A multilinear isotropic hardening material model is used to simulate the elastoplastic forming of the inner tie-rod end stud, with the inner ball and mold discretized using ten-node solid elements. The isotropic hardening model captures monotonic plastic flow, but does not account for Bauschinger effects during unloading, which may affect absolute stress magnitudes.

Frictional contact is defined between the stud and the mould, as well as between the stud and the inner ball. The POM bearings and the ball are modeled as a single piece due to the complexity of the nonlinear problem, which includes both contact and material nonlinearity. The coefficient of friction between the stud and the mould is set to 0.18, whereas it is 0.22 between the stud and the inner ball, considering the presence of the POM bearings [6]. The mesh sensitivity analysis incorporates element quality, aspect ratio, and computational efficiency. The final model comprises 26.110 3D tetrahedral elements. The mesh configuration, boundary conditions, and contact definitions are illustrated in Figure 6. The displacement-based modeling approach is applied to the boundary conditions, and the stud forming displacement is determined by considering the stud's inner dimensions, which are crucial for the free rotation of the end ball supported by POM. The tie end is free to move in the forming direction, whereas the mold is fixed. The mechanical properties of the inner tie-rod end studs are given in Table 1 [29-30].

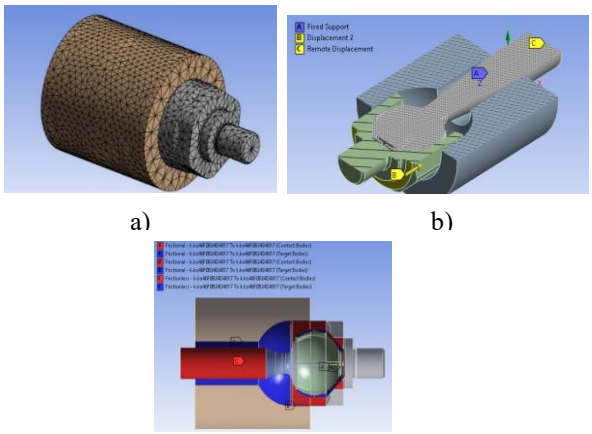


a) b)

c)

Figure 6. Inner tie-rod end stud forming process finite element model, a) Mesh, b) Boundary conditions

c) Contact surfaces

The strain hardening exponent and strength coefficient in the table were obtained from the true stress–strain curve using the Hollomon equation below.

$$\sigma_T = K\,\varepsilon^n \qquad (1)$$

The strength coefficient and the strain hardening coefficient in Table 1 were obtained using linear regression with the least squares method [31].

Table 1. The mechanical properties of the inner tie-rodend stud

| Materials | Yield Strength (MPa) | Tensile Strength (MPa) | Elongation (%) | Strength Coefficient K (MPa) | Hardening Coefficient n |
|---|---|---|---|---|---|
| SAE 1040 | 250 | 625 | 15 | 1295 | 0.29 |
| 16MnCr5 | 390 | 510 | 19 | 672 | 0.13 |

The table shows that SAE 1040 exhibits lower strength and higher strain hardening, meaning it work-hardens more, with reduced ductility.

## Finite Element Analysis Results

A nonlinear finite element analysis was carried out to examine the forming response of the inner tie-rod end stud. Initially, the effect of material selection (SAE 1040 and 16MnCr5) on axial expansion and residual stress distribution was assessed through comparison with experimental measurements. Subsequently, a wrench-size-based design modification was analyzed for SAE 1040 to mitigate axial expansion. The FEA results, including axial displacement and residual equivalent (Von Mises) stress distributions governed by the free rotation of the POM-supported ball end and the internal geometry of the stud, are presented in Figures 7–10.

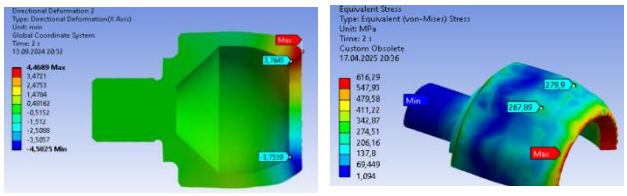

a) b)

Figure 7. Inner tie-rod end stud FEA results (SAE 1040) a) Axial displacement b) Residual equivalent stress

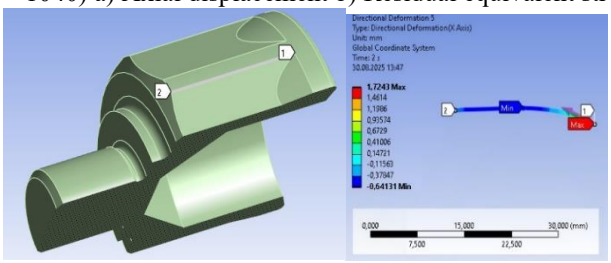

Figure 8. FEA axial expansion results at the outer side of the inner tie-rod end stud wrench (SAE 1040)

The inner diameter results at the formed edge section show good agreement with the experimental findings. In SAE 1040, however, strain localization at the wrench corner leads to residual equivalent stresses approaching the tensile strength, explaining the excessive deformation observed experimentally.

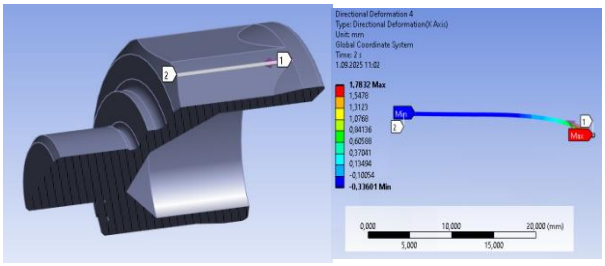

Figure 9. Inner tie-rod end stud FEA results (16MnCr5)

a) Axial displacement b) Residual equivalent stress

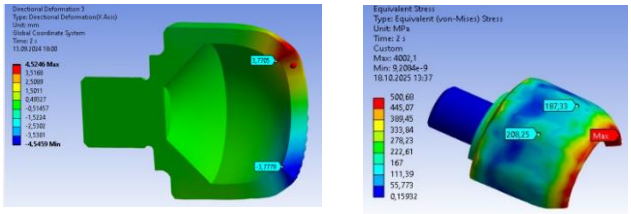

a) b)

Figure 10. FEA axial expansion results at the outer side of the inner tie-rod end stud wrench (16MnCr5)

The axial expansion in SAE 1040 is approximately twice that of 16MnCr5, consistent with the higher von Mises stress levels that exceed the yield strength and promote plastic localization. Accordingly, Figure 11 presents the plastic residual strains at the critical points after elastic strain recovery, confirming the greater plastic strain accumulation in SAE 1040.

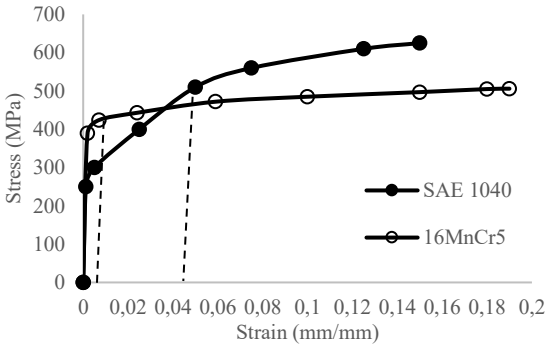


Figure 11. The plastic residual strains obtained after elastic strain recovery at critical points

The effects of material on the forming behavior of the inner tie-rod end stud are summarized in Table 2, where the

internal diameter after forming is denoted as $D_{INT}$, with the subscripts "EXP" and "FEA" referring to the experimental and finite element analysis results, respectively. Axial expansion in the experiments and FEA simulations is denoted by $\delta_Z$ measured along the z-axis. The residual equivalent stresses at the critical expansion zone and the formed edge zone are denoted by $\sigma_{VM,CRT}$, $\sigma_{VM,EDGE}$ respectively. The second stage of the analysis focuses on the wrench-size-based design of the inner tie-rod end stud made of SAE 1040, prompted by the axial expansion observed in both experiments and finite element analysis. The Figures 12–13 below illustrate the residual equivalent stress and axial expansion results for Design 2 and Design 3, respectively, as referenced in Figure 3. Table 3 summarizes the expansion and residual stresses at the critical expansion zone and the edge zone for all designs.

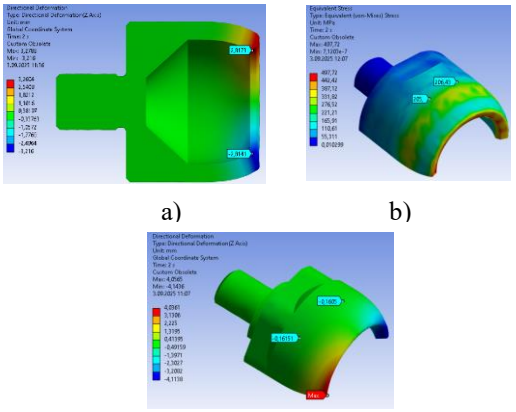

a) b)

c)

Figure 12. Inner tie-rod end stud FEA results for design 2

a)Axial displacement at the inner side b) Residual equivalent stress at the expansion zone
c) Axial expansion results

The internal diameter was selected as the primary reference parameter because it represents the functional contact surface of the rod head; dimensional accuracy governs load transfer and assembly tolerances. Axial expansion deviations observed in some configurations arise from contact interaction, geometric nonlinearity, and material hardening. The material behavior was modeled using an isotropic hardening model; Bauschinger effects during unloading, along with the assumptions of constant friction and simplified contact stiffness, may affect local stress peaks. While the model reliably captures deformation trends and localization, absolute stress magnitudes should be interpreted considering these limitations.

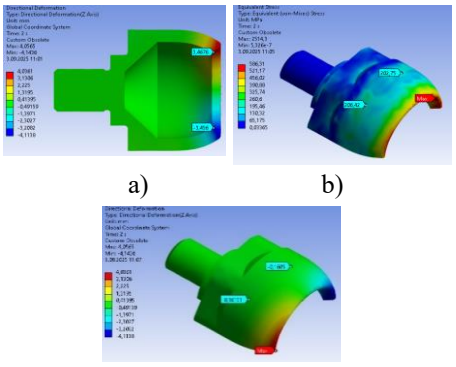

a) b)

c)

Figure 13. Inner tie-rod stud FEA results for design 3

a) Axial displacement at the inner side b) Residual equivalent stress at the expansion zone c) Axial expansion results

Shortening the wrench size in Designs 2 and 3 reduces the geometric restriction of plastic flow at the flat–corner transition, thereby limiting strain localization and triaxial stress development compared to Design 1. As a result, plastic strain accumulation, residual stresses, and axial expansion decrease, consistent with the lower plastic strain shown in Figure 14

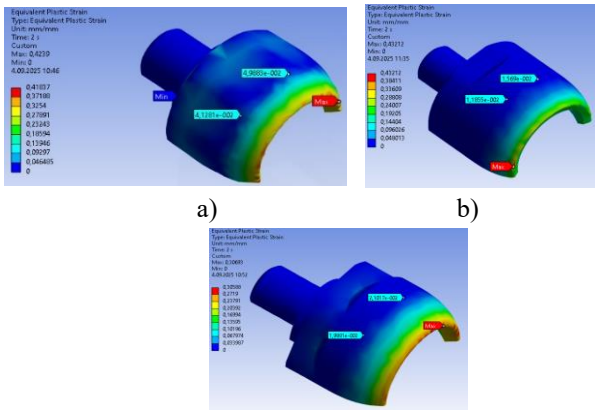

a) b)

c)

Figure 14. Equivalent plastic strains a) Design 1 a) Design 2 c) Design 3

Table 2. The effects of material on the forming results of the inner tie-rod end stud (Design 1)

| Material | $D_{INT,EXP}$ (mm) | $D_{INT,FEA}$ (mm) | Error % | $\delta_{Z,EXP}$ (mm) | $\delta_{Z,FEA}$ (mm) | Error % | $\sigma_{VM,CRT}$ (MPa) | $\sigma_{VM,EDGE}$ (MPa) |
|---|---|---|---|---|---|---|---|---|
| SAE 1040 | 23.50 | 23.66 | 0.67 | 1.05 | 1.28 | 17.96 | 270 | 616 |
| 16MnCr5 | 23.50 | 23.62 | 0.50 | - | 0.22 | 22 | 208 | 500 |

Table 3. The effects of design on the forming results of the inner tie-rod end stud (Material 1)

| Design Number | $D_{INT,EXP}$ (mm) | $D_{INT,FEA}$ (mm) | Error % | $\delta_{Z,EXP}$ (mm) | $\delta_{Z,FEA}$ (mm) | Error % | $\sigma_{VM,CRT}$ (MPa) | $\sigma_{VM,EDGE}$ (MPa) |
|---|---|---|---|---|---|---|---|---|
| Design 1 | 23.55 | 23.66 | 0.46 | 1.05 | 1.28 | 17.96 | 270 | 616 |
| Design 2 | 25.83 | 25.40 | 1.66 | 0.38 | 0.30 | 21.05 | 205 | 497 |
| Design 3 | 24.23 | 24.24 | 0.04 | 0,22 | 0.32 | 31.25 | 206 | 586 |

The plastic strains at the formed end section exceeded the material's ductility limit for SAE 1040, leading to localized plastic deformation observed in the manufactured specimens, as shown in Figure 15.

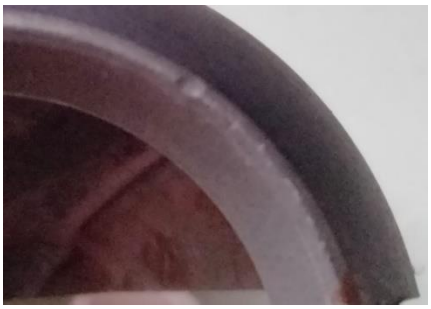

Figure 15. Forming-induced plastic deformation in the tie-rod end formed section

The plastic deformation at the formed end region is manifested as a localized plastic strain concentration, without any evidence of macroscopic cracking or fracture, showing good agreement with the equivalent plastic strain distribution obtained from FEA.

## Microstructure and Microhardness Examination

After forming, the inner tie-rod end stud was mechanically split into two sections to facilitate measurement of the formed and unformed regions for two materials. The chemical compositions of steels, which are provided as hot-rolled round bars from producers, are given in Table 4.

Table 4. Chemical composition of steels in the forming process according to EN 10204 standards

| Material | C | Si | Mn | Cr | Cu | Ni | Mo |
|---|---|---|---|---|---|---|---|
| SAE 1040 | 0.43 | 0.25 | 0.70 | 0.13 | 0.08 | 0.07 | 0.03 |
| 16MnCr5 | 0.16 | 0.23 | 1.01 | 0.85 | 0.08 | 0.06 | 0.02 |

Microstructural analysis of the formed and unformed sections of the inner tie-rod end stud (Figures 16–17) was conducted to evaluate phase constitution and grain orientation. SAE 1040 and 16MnCr5 are low- to medium-carbon steels; however, they serve different applications and contain distinct alloying elements that influence their microstructural characteristics. Furthermore, microstructural evolution is significantly affected by hot rolling conditions through cooling transformation kinetics [32]. SAE 1040 has a higher carbon content compared to 16MnCr5, which results in a higher fraction of pearlite in its microstructure, as seen in the figures. Brittle pearlite lamellae are commonly observed in steels with 0.2–0.4% carbon content [33].

The higher carbon content of SAE 1040 makes it less ductile than 16MnCr5 and more prone to cracking during cold forming, due to its higher pearlite content. As observed from the figures, 16MnCr5 exhibits superior forming capability, characterized by a higher degree of grain orientation compared to SAE 1040.

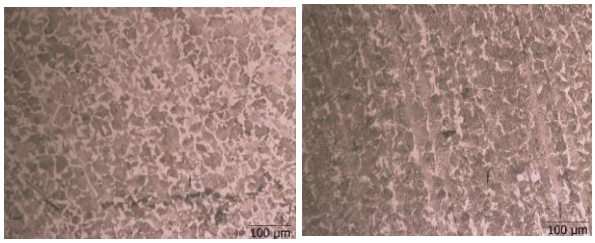


a) b)

Figure 16. SAE 1040 microstructure a) Unformed section b) Formed end section

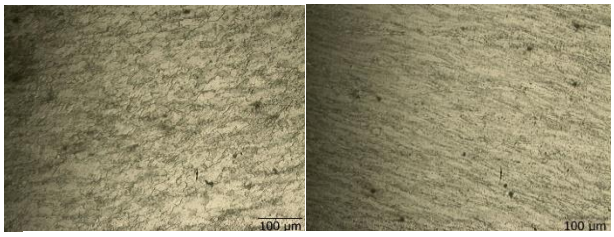


a) b)

Figure 17. 16MnCr5 Microstructure a) Unformed section b) Formed end section

Microhardness analyses were performed to evaluate strain hardening behavior and localized plastic deformation mechanisms, as shown in Figure 18. No evidence of macroscopic cracking or catastrophic fracture was observed in the specimens; however, localized plastic deformation reaching the strain limit occurred at the edge sections. The higher hardness of SAE 1040 steel is attributed to its carbon content, and both steels exhibit strain hardening due to plastic deformation during forming. The higher hardening rate of SAE 1040 is consistent with its strain hardening coefficient and the microhardness measurements.

Residual plastic strain accumulation, together with the

lower yield strength and ductility of SAE 1040, contributes to the observed non-uniform expansion, particularly within the plastic zone, compared with 16MnCr5.

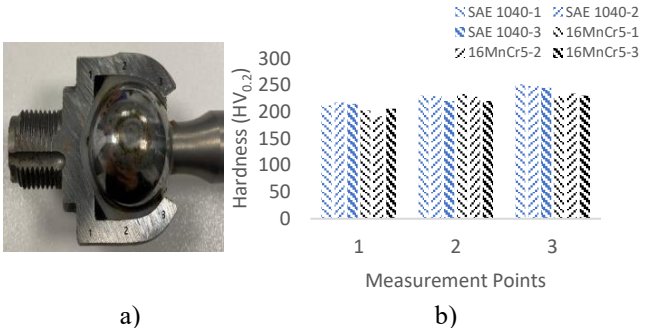


a) b)

,Figure 18. Microhardness measurements of inner tie-rod end stud: a) Measurement points b) Microhardness $Hv_{0.2}$ results

The non-uniform expansion behavior in SAE 1040 is further supported by hardness variations consistent with its hardening coefficient. In contrast, 16MnCr5 exhibits a more uniform hardness distribution while maintaining superior forming capability relative to SAE 1040.

## Conclusions

In this study, the forming analysis of the inner tie-rod end stud was conducted both numerically and experimentally. The finite element analysis results demonstrate that the displacement-based implicit finite element model, incorporating material and contact nonlinearities, accurately predicts forming-induced expansion behavior. Microstructural analysis indicates a higher pearlite fraction in SAE 1040 steel compared with 16MnCr5, leading to reduced formability in the former. The combined experimental and numerical results reveal that material expansion occurs in SAE 1040 steel, with stress concentration at the wrench corners further intensifying this behavior, unlike in 16MnCr5.

The lower yield strength of SAE 1040 steel and the accumulation of residual plastic strains promote material expansion at the peak region under unloading conditions, which is undesirable for serial production. Residual plastic strains generated during forming are identified as the primary driver of post-forming axial expansion, while earlier plastic localization at the wrench corners accelerates strain accumulation. Upon unloading, incomplete elastic recovery results in elevated residual stresses and measurable dimensional expansion. Forming-induced strain hardening and the associated reduction in ductility are shown to govern material hardness and strain localization in the formed end regions, with the hardening rate derived from the Hollomon equation exhibiting strong agreement with microhardness measurements.

Implementation of the wrench-size-based design modification yields an approximately one-third reduction in material expansion compared with the initial configuration, consistent with the plastic strain analysis. However, expansion is not completely eliminated, indicating that geometric modification alone is insufficient to achieve full dimensional accuracy for SAE 1040. These findings highlight the critical role of material selection and local geometric design in controlling forming-induced residual strains and dimensional deviations, providing practical guidance for manufacturing-oriented design optimization and process parameter adjustment in steering component production.

## Ethics committee approval and conflict of interest statement

There is no conflict of interest with any person/institution in the article prepared.

## Authors' Contributions

Model preparation, finite element analysis: Eruslu & Kölemen.

Study conception, preparation of manuscript: Eruslu & Kahraman.

Production of forming stud samples, measurement of forming stud samples: Kölemen

Microhardness and microstructural measurements: Kahraman & Eruslu.

## Acknowledgment

This study was funded by SIO Automotive A.Ş. through the Research Project No: RD24-1.

## References

[1] M. Z. Okur and D. A. Bircan, "Design and simulation of a heavy-duty vehicle steering component by analytic and FEA method," *Eurasian Journal of Science, Engineering and Technology*, vol. 2, no. 1, pp. 1–9, 2021.

[2] A. H. Falah, M. A. Alfares and A. H. Elkholy, "Failure investigation of a tie-rod end of an automobile steering system," *Engineering Failure Analysis*, vol. 14, pp. 895–902, 2007, doi:10.1016/j.engfailanal.2006.11.045.

[3] O. Ikechukwu, E. O. Ebunilo, and E. Ikpe, "Investigation of a vehicle tie-rod failure in relation to the forces acting on the suspension system," *American Journal of Engineering Research*, vol. 5, no. 6, pp. 208–217, 2016.

[4] W. Duan and S. Joshi, "Analysis of threaded connections in large-scale steel tie rods," *Engineering Failure Analysis*, vol. 18, pp. 2008–2018, 2011, doi:10.1016/j.engfailanal.2011.06.002.

[5] S. K. Koh, "Fatigue analysis of an automotive steering link," *Engineering Failure Analysis*, vol. 16, pp. 914–922, 2009, doi:10.1016/j.engfailanal.2008.08.014.

[6] M. Ozsoy and M. K. Pehlivan, "Computer-aided structural analysis of a tie-rod end," *Acta Physica Polonica A*, vol. 128, no. 2-B, pp. 488–490, 2015, doi:10.12693/APhysPolA.128.B-488.

[7] A. J. Godase and P. P. Kulkarni, "Tie rod design and analysis: A review," *International Journal of Current*

*Engineering and Technology*, vol. 7, no. 6, pp. 2046–2050, 2017.

[8] I. N. Budak and M. Pekedis, "Plastik şekil değişimine uğramış otomobil rotunun yorulma davranışının deneysel ve sayısal analizi," *Dokuz Eylül Üniversitesi Fen ve Mühendislik Dergisi*, vol. 23, no. 68, pp. 647–659, 2021, doi:10.21205/deufmd.2021236826.

[9] K. Polat, M. M. Topac and F. Çoban, "Effect of design parameters on buckling tendency of an eccentric drag link used in a truck steering linkage: A DOE/RSM-based design optimisation study," *Journal of Automotive Science and Technology*, vol. 8, no. 3, pp. 387–396, 2024, doi:10.30939/ijastech.1484736.

[10] P. M. Chavan and M. M. M. Patnaik, "Performance evaluation of passenger car tie rod using numerical and theoretical approach with different materials," *International Journal of Research in Engineering and Technology*, vol. 3, no. 8, pp. 92–100, 2014, doi:10.15623/IJRET.2014.0308015.

[11] P. R. Vithalkar and R. R. Gawande, "Study of analysis of bus passenger tie rod: A review," *International Journal of Research in Engineering and Technology*, vol. 4, no. 11, pp. 239–241, 2015, doi:10.15623/IJRET.2015.0411041.

[12] E. Uludamar, S. G. Biçer and M. Taş, "Sonlu elemanlar metodu kullanılarak rot üzerinde oluşan gerilmelerin hesaplanması," *Adana Bilim ve Teknoloji Üniversitesi Fen Bilimleri Dergisi*, vol. 1, no. 2, pp. 30–35, 2018.

[13] L. Zang and E. Dong, "Dynamics simulation on vehicle steering mechanism," in *Proc. 2nd Int. Conf. Electronic & Mechanical Engineering and Information Technology*, 2012, pp. 1952–1955, doi:10.2991/emeit.2012.432.

[14] I. A. Essienubong, O. Ikechukwu, P. O. Ebunilo, and E. E. Ikpe, "Static analysis on a vehicle tie rod to determine the resulting buckling displacement," *International Journal of Industrial and Manufacturing Systems Engineering*, vol. 1, no. 1, pp. 16–24, 2016, doi:10.11648/j.ijimse.20160101.13.

[15] H. Basak, "Outer tie rod design by using topology optimization, analysis and verification," *Journal of Polytechnic*, vol. 27, no. 3, pp. 1055–1068, 2024, doi:10.2339/politeknik.1198353.

[16] A. Diaz et al., "Residual stresses in cold-formed steel members: Review of measurement methods and numerical modelling," *Thin-Walled Structures*, vol. 159, 2021, doi:10.1016/j.tws.2020.107335.

[17] R. H. Wagoner and J. L. Chenot, *Metal Forming Analysis*. Cambridge, UK: Cambridge University Press, 2005, doi:10.1017/CBO9781139087070.

[18] S. Kobayashi, S. I. Oh and T. Altan, *Metal Forming and the Finite-Element Method*. Oxford, UK: Oxford University Press, 1989.

[19] E. Oñate et al., *Advances in Computational Plasticity*. Cham, Switzerland: Springer, 2017, doi:10.1007/978-3-319-60885-3.

[20] J. Riháček and L. Mrňa, "Comparison of implicit and explicit algorithms of finite element method for the numerical simulation of hydroforming process," *MM Science Journal*, pp. 1326–1331, 2016, doi:10.17973/MMSJ.2016_11_2016114.

[21] B. B. He et al., "High dislocation density-induced large ductility in deformed and partitioned steels," *Science*, vol. 357, pp. 1029–1032, 2017, doi:10.1126/science.aan0177.

[22] W. M. Quach and P. Qiu, "Strength and ductility of corner materials in cold-formed stainless-steel sections," *Thin-Walled Structures*, vol. 83, pp. 28–42, 2014, doi:10.1016/j.tws.2014.01.020.

[23] E. Schafler et al., "Dislocation densities and internal stresses in large strain cold worked pure iron," *Materials Science and Engineering A*, vol. 234–236, pp. 445–448, 1997, doi:10.1016/S0921-5093(97)00168-8.

[24] R. Su et al., "Factors influencing residual stresses in cold expansion and their effects on fatigue life: A review," *Coatings*, vol. 13, no. 12, pp. 1–23, 2023, doi:10.3390/coatings13122037.

[25] Z. Marciniak, J. L. Duncan and S. J. Hu, *Mechanics of Sheet Metal Forming*. Oxford, UK: Elsevier, 2002, doi:10.1016/b978-0-7506-5300-8.x5000-6.

[26] T. X. Yu and W. Johnson, "Influence of axial force on the elastic-plastic bending and springback of a beam," *Journal of Materials Processing Technology*, vol. 6, pp. 5–21, 1982, doi:10.1016/0378-3804(82)90016-X.

[27] S. L. Zang et al., "A model of one-surface cyclic plasticity and its application to springback prediction," *International Journal of Mechanical Sciences*, vol. 53, pp. 425–435, 2011, doi:10.1016/j.ijmecsci.2011.03.005.

[28] R. H. Wagoner, H. Lim and M. G. Lee, "Advanced issues in springback," *International Journal of Plasticity*, vol. 45, pp. 3–20, 2013, doi:10.1016/j.ijplas.2012.08.006.

[29] O. Aydin and C. Simsir, "Application of the contour method to determine axial residual stresses in cold extruded steel rods," *FME Transactions*, vol. 49, pp. 941–949, 2021, doi:10.5937/fme2104941A.

[30] A. Calık, O. Sahin and N. Ucar, "Mechanical properties of boronized AISI steels," *Acta Physica Polonica A*, vol. 115, no. 3, pp. 694–698, 2008, doi:10.12693/APhysPolA.115.694.

[31] R. Marangoz et al., "Hydroforming analysis of exhaust pipe connectors," *Materials Testing*, vol. 62, no. 9, pp. 901–907, 2020, doi:10.1515/mt-2020-620907.

[32] *ASM Handbook, Volume 4C: Induction Heating and Heat Treatment*. ASM International, 2014.

[33] J. P. Houin, A. Simon and G. Beck, "Relationship between structure and mechanical properties of pearlite," *ISIJ International*, vol. 21, pp. 726–731, 1980, doi:10.2355/isijinternational1966.21.726.